Temporal Characterization of Femtosecond Laser-Plasma-Accelerated Electron Bunches using THz Radiation

J. van Tilborg*,[1] C. B. Schroeder,[1] C. V. Filip,[2] Cs. Tóth,[1] C. G. R. Geddes,[1]
G. Fubiani†,[1] R. Huber,[1] R. A. Kaindl,[1] E. Esarey,[1] and W. P. Leemans[1]

[1]*Lawrence Berkeley National Laboratory,*
University of California, Berkeley, California 94720, USA
[2]*University of Nevada, Reno, Nevada 89557, USA*

(Dated: July 12, 2005)

Abstract

The temporal profile of relativistic laser-plasma-accelerated electron bunches has been characterized. Coherent transition radiation at THz frequencies, emitted at the plasma-vacuum boundary, is measured through electro-optic sampling. The data indicates that THz radiation is emitted by a skewed bunch with a sub-50 fs rise time and a $\simeq$600 fs tail (half-width-at-half-maximum), consistent with ballistic debunching of 100%-energy-spread beams. The measurement demonstrates both shot-to-shot stability of the laser-plasma accelerator and femtosecond synchronization between bunch and probe beam.

PACS numbers: 29.25.Bx, 41.60.-m, 52.38.Kd, 78.47.+p

* Also at Eindhoven University of Technology, the Netherlands.
† Also at University of Paris XI, Orsay, France.

Laser-driven plasma-based accelerators [1–9] are of great interest to the scientific community because of the ultra-high accelerating gradients generated, and the high-brightness electron bunches that are produced. In such an accelerator, a focused intense ($> 10^{19}$ W cm^{-2}) laser pulse drives a plasma density wave, oscillating at the plasma frequency. For a sufficiently large amplitude wave, plasma electrons can be trapped and accelerated to relativistic energies. Accelerating gradients on the order of 10-100 GV m^{-1}, and generation of multi-nC electron bunches have been demonstrated [3–9]. Simulations and theory [10, 11] indicate that the electron bunches are intrinsically short and dense since the transverse bunch size is on the order of the laser spotsize (~ 10 μm), and the bunch length is on the order of the plasma wavelength (typically, 5–30 μm depending on plasma density). The laser, the relativistic electrons, and secondary radiation such as gamma-rays [12], x-rays [13, 14], and THz waves [15–17] are intrinsically synchronized in time. The compact size of the accelerator, the ultra-short electron bunch generation, and the synchronized radiation emission open a broad perspective for future scientific experiments.

Temporal characterization of electron beams produced by conventional accelerators has been performed by analyzing coherent transition radiation (CTR), emitted by the electron bunch as it propagates from one medium to another [18], e.g., through a metallic foil [19–21]. For the laser-plasma accelerator [also referred to as laser-wakefield accelerator (LWFA)], the plasma-vacuum interface acts as the media transition and coherent THz radiation has been measured [15–17, 22]. Previous CTR experiments on LWFA-produced electron bunches have focused on measuring THz pulse energy and polarization [15], and two energy measurements in different spectral ranges of detector acceptance suggested the existence of laser-plasma-produced sub-100 fs bunch structure [22]. However, to date, neither extensive spectral analysis, nor temporal characterization of the THz pulse and the LWFA electron bunch profile have been realized.

In this Letter we report on THz waveform measurements (amplitude and phase), obtained with an electro-optic (EO) sampling technique [23–28], performed to derive properties of the temporal profile of the LWFA electron beam. This measurement also demonstrates LWFA stability and applicability in pump-probe type of experiments. Through the EO effect, the THz waveform induces a change in birefringence of a crystal, proportional to the electric field strength and sign, which is then probed by a second femtosecond laser beam (probe beam). By scanning the delay between the THz pulse and probe beam, a

full THz waveform was recorded. The experiments were performed with the high-power Ti:Al_2O_3 laser of the L'OASIS facility at the Lawrence Berkeley National Laboratory [22]. A schematic of the experimental configuration is shown in Fig. 1. A Ti:Al_2O_3 laser beam (wavelength of $\lambda_0 = 800$ nm) was focused [spot size $\simeq 3.6$ μm root-mean-square (rms)] by an off-axis parabola (OAP1) onto Helium gas emerging from a gas jet (diameter of 2 mm) with a backing pressure of 1000 psi. The peak electron density in the plasma was 3×10^{19} cm^{-3}, corresponding to a plasma wavelength of $\lambda_p = 6$ μm. The total charge of the electron bunch, generated during the laser-plasma interaction, was $\simeq 2.4$ nC (or 1.5×10^{10} electrons), measured 50 cm from the gas jet. The electron energy distribution $g(E)$, measured by a magnetic spectrometer and averaged over multiple shots, showed an exponential form of $g(E) \sim \exp(-E/E_t)$, with $E_t = 5$ MeV. Part of the THz radiation was collected and collimated by an F/2 90-degree off-axis parabola (OAP2, focal length of 15 cm), positioned off-centered ($\theta = 19^\circ$ with respect to the main propagation axis) to avoid damage from the electron beam or laser beam. The collimated THz radiation was then focused by an F/2.4 90-degree off-axis parabola (OAP3, focal length of 18 cm) onto a 200-μm-thick ZnTe crystal, positioned outside the target chamber [a 3.2-mm-thick polyethylene (PE) disk served as window]. A high-resistivity Si wafer blocked remnant laser light from interfering with the EO detection. A 21-fs (rms) Ti:Al_2O_3 probe beam, split off from the main laser beam to provide synchronization, was focused (spotsize < 20 μm) to overlap with the THz beam in the ZnTe crystal. A polarizer set the polarization of the probe beam to horizontal (i.e. p), while the analyzer was rotated to transmit only the vertical component to a biased photo-diode (Diode). The ZnTe crystal is cut in the $\langle 110\rangle$-plane, and the $\langle 001\rangle$-axis was rotated to optimize the signal-to-noise ratio of the EO measurement. The electric field vectors of the probe beam and THz pulse are shown in the bottom right of Fig. 1. Although the emitted THz pulse is radially polarized [16], OAP2 selects a specific polarization component which corresponds to vertical polarization at the crystal surface.

With future single-shot EO experiments as a motivation, single-diode detection of the probe beam [29] was preferred over balanced-diode detection [23]. To resolve the sign of the THz pulse, a quarter-wave-plate ($\lambda/4$–plate) was used to provide the necessary ellipticity to the probe beam polarization. It has been shown [29] that in this case (sign-resolved single-diode EO sampling), the best signal-to-noise is obtained with a small rotation of the $\lambda/4$–plate (in this experiment by 5°), such that near-zero optical transmission is realized.

The THz wave will modify the probe beam ellipticity by a phase retardation $\Delta\phi$, and cause an increase or decrease of the transmitted probe beam energy $T_{\mathrm{EO}}(\tau)$, depending on the time delay τ between probe beam and THz pulse. For THz fields of equal but opposite magnitude, the change in transmission is not symmetric (not identical), but a well-known function of probe beam ellipticity [29]. For this reason the transmission measurement $T_{\mathrm{EO}}(\tau)$ was symmetrized using this function, yielding the EO signal $S_{\mathrm{EO}}(\tau)$.

There are several other EO-related effects that influence THz waveform analysis [28, 30]: (1) The probe beam has a finite pulse length, limiting the temporal resolution of the EO method. (2) Dispersion and absorption in the ZnTe crystal causes THz pulse distortion. (3) There is a mismatch between the phase velocity of the individual THz frequencies and the group velocity of the probe beam. Since the ZnTe crystal has a well characterized dispersion function in both the near-infrared and THz spectral domain [28, 31, 32], these effects can be modeled and the original THz waveform $E_{\mathrm{THz}}(t)$ can be extracted from the measured (and symmetrized for probe beam ellipticity) EO signal $S_{\mathrm{EO}}(\tau)$. In the frequency domain, a slowly varying envelope approximation can be applied to the convolution of the probe beam and the THz waveform [30], yielding

$$S_{\mathrm{EO}}(\omega) \sim r_{41}(\omega) I_{\mathrm{pr}}(\omega) E_{\mathrm{THz}}(\omega) T_{\mathrm{ZnTe}}(\omega), \tag{1}$$

with $\omega = 2\pi\nu$ the angular frequency, $I_{\mathrm{pr}}(\omega) = e^{-\omega^2\sigma_{\mathrm{pr}}^2/4}$, σ_{pr} the probe beam pulse length (rms), and $r_{41}(\omega)$ the EO coefficient. The crystal transfer function $T_{\mathrm{ZnTe}}(\omega)$ incorporates the dispersion, absorption, and mismatch in the ZnTe crystal. The inset in Fig. 2 shows the amplitude of the ZnTe transfer function (solid curve), the spectrum of the envelope of the probe beam $e^{-\omega^2\sigma_{\mathrm{pr}}^2/4}$ (dotted curve), as well as the theoretical curve for CTR from a 50-fs (rms) Gaussian electron bunch (dashed curve). Above 4 THz, the 200-μm-thick crystal effectively operates as a cut-off filter, mainly due to the mismatch between both beams.

The CTR characteristics can be modeled from the well-known angular and spectral distribution function for an electron passing a metal-vacuum boundary [18]. Concerning the LWFA, previous analysis [16] has shown that the plasma-vacuum boundary can be modeled as a metal-vacuum interface with a finite transverse size given by the transverse extent of the plasma. To include the coherence effects at the boundary, the angular and spectral distribution function is multiplied by the form factor $F(\omega)$ of the electron bunch and by the diffraction function $D(\omega)$ [16], such that the differential energy per unit bandwidth $d\omega$ and

unit solid angle $d\Omega$ is

$$\frac{d^2W}{d\omega d\Omega} \sim \left| \int g(u) \frac{u\sqrt{1+u^2}\sin\theta}{1+u^2\sin^2\theta} D(\omega,u) F(\omega,u) du \right|^2 , \tag{2}$$

where θ is the angle of emission with respect to the electron propagation axis, and $g(u)$ is the electron momentum distribution with u the electron momentum normalized to $m_e c$. CTR from a mono-energetic distribution at $u = u_t$ closely approximates CTR from an electron bunch with Boltzmann distribution $g(u) \sim \exp(-u/u_t)$ [17]. In the experimental setup, the angle of observation was $\theta = 19°$, and electron energy measurements yielded a normalized momentum $u_t \simeq 10$. The CTR spectrum in the inset of Fig. 2 (dashed curve) is derived from a Gaussian electron bunch with a length (rms) of 50 fs, exiting a plasma with transverse radius of $\rho = 100$ μm (consistent with plasma density interferometry). The ZnTe-induced EO signal $S_{\rm EO}(\tau)$ from this bunch form, with $S_{\rm EO}(\tau)$ the inverse Fourier transformation of $S_{\rm EO}(\omega)$, is plotted as a solid curve in the main plot of Fig. 2. The dashed curve in the same plot indicates the EO signal through use of an ideal crystal (no mismatch, no dispersion, no absorption and an ultra-short probe beam). The reflective THz losses at the crystal interface only significantly affect the amplitude of $S_{\rm EO}(\tau)$, and not the shape of the waveform, and are therefore ignored here.

The EO measurement, which is representative for several data-sets, is shown in Fig. 3(a) as grey dots, where the measured EO signal $S_{\rm EO}(\tau)$ is plotted versus time delay. The delay stage was scanned with steps of 20 fs, and at each step 10 laser shots were taken, resulting in a 60-minute long scan at 0.4 Hz system operation. The error bars represent the standard deviation on the 10 shots. The Fourier transformation of the data is plotted as grey dots in Fig. 3(b). A combination of shot-to-shot fluctuations in probe-beam parameters and accelerator performance can contribute to noise on the EO measurement. Since a clean EO waveform was recorded in this single-diode EO configuration (no reference diode), where frequencies up to the 200-μm-thick ZnTe detection limit of 4 THz were fully resolved, a stable accelerator performance was demonstrated.

Figures 3(a) and 3(b) also display the modeled EO signal $S_{\rm EO}(\tau)$ (solid black curve) based on CTR from a skewed electron beam profile. A good fit with the data is obtained for a skewed electron bunch with a rise time of 50 fs, and a tail of 600 fs [half-width-at-half-maximum (HWHM)]. Since the ZnTe crystal has a spectral cut-off above 4 THz, the rising edge could be shorter than 50 fs without significantly modifying the measured EO signal.

However, if a longer rising edge is chosen, the theoretical curve no longer agrees with the measured sharp spectral cut-off at 4 THz. Fig. 3(c) shows the EO signal fit on the data if, instead of a skewed bunch-form, a Gaussian charge distribution (rms of 50 fs) is assumed. Note that the Gaussian fit does not match the negative peaks of the measured waveform; this discrepancy supports the presence of a longer electron tail (which will reduce the back of the EO signal).

Two mechanisms can contribute to the skewed electron distribution, both related to the finite-size longitudinal density ramp at the exit of the plasma: (1) As the electron bunch propagates down the ramp, and before it reaches the CTR emission-interface [16], ballistic motion of the 100%-energy-spread bunch, combined with space-charge interaction, result in a higher-energy, sharp electron front [33]. (2) At the falling edge of the density ramp, the plasma wavelength increases causing the phase velocity of the plasma wave to decrease, and trapping of lower-energy electrons several plasma wavelengths behind the laser-pulse, and behind the leading higher-energy bunch is realized [34, 35]. More detailed knowledge on the plasma density profile, as well as theoretical understanding of electron trapping and propagation through the ramp, are necessary to correlate CTR measurements to the evolving six-dimensional electron distribution function.

An additional data-set with a linear polarization state of the probe beam was recorded. In this measurement, the peak diode signal (maximal EO effect) showed a transmission of $T_{\mathrm{EO}} = 5.7 \times 10^{-3}$, where $T_{\mathrm{EO}} = 1$ represents the total energy in the probe beam. The peak phase retardation $\Delta\phi$, induced by the THz pulse, is related to the peak transmission through $\Delta\phi \simeq 2\sqrt{T_{\mathrm{EO}}}$, resulting in $\Delta\phi \simeq 0.15$ rad. $\Delta\phi$ can be related to the incident peak THz field [24] through $\Delta\phi = 2\pi L n_0^3 r_{41} E_{\mathrm{THz}}/(\lambda_0\sqrt{\eta})$, with $n_0 = 2.85$ the refractive index for ZnTe at $\lambda_0 = 800$ nm, r_{41} the EO coefficient ($r_{41} \simeq 4.0 \times 10^{-12}$ m V^{-1} [36]), and $\eta \simeq 3$–6 the EO transmission reduction due to THz reflection at the crystal surface and THz pulse distortion in the ZnTe. One finds that the incident peak field was in the range between $E_{\mathrm{THz}} = 18$–25 kV cm^{-1}.

Since OAP2 collects less than 5% of the originally radially-polarized THz beam, higher peak fields could be realized through improved collection in future experiments. Furthermore, the generation of high-energy (> 100 MeV) quasi-mono-energetic and low-divergence electron beams in a channel-guided LWFA, which has recently been demonstrated [8], could significantly boost peak fields of femtosecond THz (CTR) pulses. In such an experiment,

CTR could be generated by propagating the electrons through a metallic foil (with reduced diffraction effects) down-stream of the gas-jet, and since the CTR generation plane is spatially separated from the gas jet and remnant laser light, efficient THz collection can be realized. Debunching due to ballistic and space-charge effects is minimal for these low-energy-spread ultra-relativistic electron beams.

In summary, temporal characterization of laser-wakefield accelerated electron bunches has been performed through single-diode EO sampling of THz radiation, emitted by the electron bunch as it passes the plasma-vacuum interface. A good fit with the data is realized by assuming bunches with a skewed charge profile, containing a sharp $\lesssim 50$ fs rising edge and a longer 600-fs tail (HWHM). The rise time could be shorter, but the measurements are limited by the temporal resolution of the 200-μm-thick ZnTe crystal. The longer tail is to be expected from propagation of 100%-energy-spread energy bunches down the plasma ramp, before the THz emission occurs. The shot-to-shot synchronization between electron and probe beam, combined with the stability of the electron beam properties are of sufficient performance to fully resolve CTR frequencies up to the 200-μm-thick ZnTe detection limit of 4 THz. Peak electric fields of the THz pulse in the range between 18–25 kV cm^{-1} were observed.

The authors gratefully acknowledge contributions from J. Byrd, M. Martin and Z. Hao on THz detection. This work was supported by the Office of Science, High Energy Physics, U.S. Department of Energy under Contract No. DE-AC03-76SF0098.

[1] T. Tajima and J. M. Dawson, Phys. Rev. Lett. **43**, 267 (1979).

[2] E. Esarey *et al.*, IEEE Trans. Plasma Sci. **24**, 252 (1996).

[3] A. Modena *et al.*, Nature **377**, 606 (1995).

[4] A. Ting *et al.*, Phys. Plasmas **4**, 1889 (1997).

[5] V. Malka *et al.*, Science **298**, 1596 (2002).

[6] W. P. Leemans *et al.*, Phys. Rev. Lett. **89**, 174802 (2002).

[7] S. P. D. Mangles *et al.*, Nature **431**, 535 (2004).

[8] C. G. R. Geddes *et al.*, Nature **431**, 538 (2004).

[9] J. Faure *et al.*, Nature **431**, 541 (2004).

[10] K.-C. Tzeng, W. B. Mori, and T. Katsouleas, Phys. Rev. Lett. **79**, 5258 (1997).

[11] E. Esarey *et al.*, Phys. Rev. Lett. **80**, 5552 (1998).

[12] W. P. Leemans *et al.*, Phys. Plasmas **8**, 2510 (2001).

[13] E. Esarey *et al.*, Phys. Rev. E **65**, 056505 (2002).

[14] A. Rousse *et al.*, Phys. Rev. Lett. **93**, 135005 (2004).

[15] W. P. Leemans *et al.*, Phys. Rev. Lett. **91**, 074802 (2003).

[16] C. B. Schroeder *et al.*, Phys. Rev. E **69**, 016501 (2004).

[17] J. van Tilborg *et al.*, Laser Part. Beams **22**, 415 (2004).

[18] M. L. Ter-Mikaelian, *High-energy electromagnetic processes in condensed media* (Wiley, New York, 1972).

[19] U. Happek, A. J. Sievers, and E. B. Blum, Phys. Rev. Lett. **67**, 2962 (1991).

[20] Y. Shibata *et al.*, Phys. Rev. E **50**, 1479 (1994).

[21] P. Kung *et al.*, Phys. Rev. Lett. **73**, 967 (1994).

[22] W. P. Leemans *et al.*, Phys. Plasmas **11**, 2899 (2004).

[23] J. A. Valdmanis, G. Mourou, and C. W. Gabel, Appl. Phys. Lett. **41**, 211 (1982).

[24] A. Yariv, *Quantum Electronics* (Wiley, New York, 1988).

[25] X. Yan *et al.*, Phys. Rev. Lett. **85**, 3404 (2000).

[26] I. Wilke *et al.*, Phys. Rev. Lett. **88**, 124801 (2002).

[27] G. Berden *et al.*, Phys. Rev. Lett. **93**, 114802 (2004).

[28] J. Faure *et al.*, Opt. Quant. Elec. **36**, 681 (2004).

[29] Z. Jiang *et al.*, Appl. Phys. Lett. **74**, 1191 (1999).

[30] G. Gallot and D. Grischkowsky, J. Opt. Soc. Am. B **16**, 1204 (1999).

[31] G. Gallot *et al.*, Appl. Phys. Lett. **74**, 3450 (1999).

[32] D. T. F. Marple, J. Appl. Phys. **25**, 539 (1964).

[33] G. Fubiani *et al.*, in *Proceedings of the 2002 Advanced Accelerator Concepts Workshop*, edited by C. E. Clayton and P. Muggli (Amer. Inst. Phys., New York, 2002), Vol. 647, pp. 203–212.

[34] S. Bulanov *et al.*, Phys. Rev. E **58**, R5257 (1998).

[35] P. Tomassini *et al.*, Phys. Rev. ST Accel. Beams **6**, 121301 (2003).

[36] Q. Wu and X.-C. Zhang, Appl. Phys. Lett. **68**, 1604 (1996).

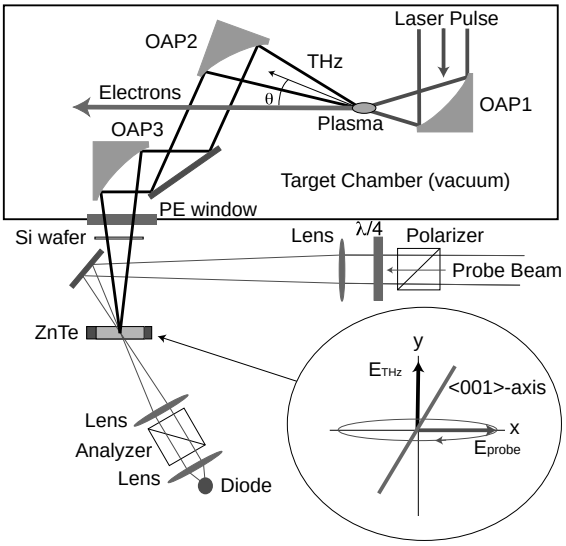

FIG. 1: Schematic representation of the laser-wakefield accelerator (LWFA), the THz (CTR) beam path, and the EO detection setup.

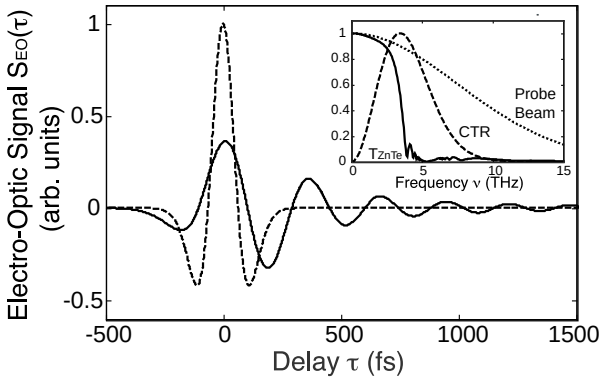

FIG. 2: The main plot shows the modeled ZnTe-induced EO signal $S_{\rm EO}(\tau)$ (solid curve), and $S_{\rm EO}(\tau)$ using a dispersion-, absorption-, and mismatch-free crystal (dashed curve). In this model, the THz radiation is CTR from a 50-fs (rms) Gaussian electron bunch. The inset shows the amplitude of the CTR spectrum (dashed curve), as well as the ZnTe transfer function $T_{\rm ZnTe}(\nu)$ (solid curve), and spectrum of the envelope of the probe beam (dotted curve).

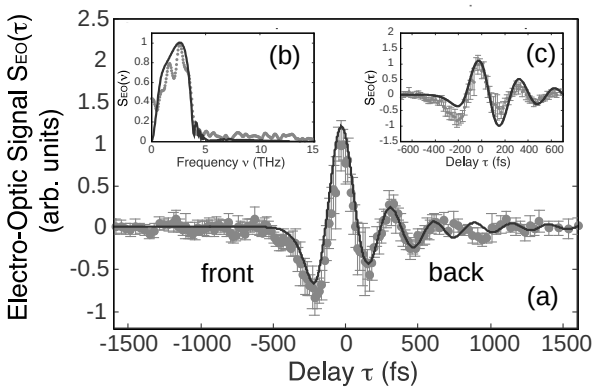

FIG. 3: The main plot (a) shows the measured EO signal $S_{\rm EO}(\tau)$ (grey dots), with the solid black line representing the modeled EO signal based on CTR from a skewed electron profile with a 50 fs rise and a 600 fs tail (HWHM). The EO signal $S_{\rm EO}(\nu)$ in the Fourier domain is shown in inset (b). The solid curve in inset (c) shows the same data as in (a) but superimposed with a modeled EO signal $S_{\rm EO}(\tau)$ based on a 50 fs (rms) Gaussian electron profile (no skew).